

# Enantiopure Benzamidinate/Cyclooctatetraene Complexes of the Rare-Earth Elements: Synthesis, Structure, and Magnetism

Meng He,<sup>†</sup> Xiao Chen,<sup>†</sup> Tilmann Bodenstein,<sup>‡,§</sup> Andreas Nyvang,<sup>‡</sup> Sebastian F. M. Schmidt,<sup>†</sup> Yan Peng,<sup>‡,§</sup> Eufemio Moreno-Pineda,<sup>§</sup> Mario Ruben,<sup>§,||</sup> Karin Fink,<sup>\*,§</sup> Michael T. Gamer,<sup>†</sup> Annie K. Powell,<sup>\*,†,§</sup> and Peter W. Roesky<sup>\*,†</sup>

<sup>†</sup>Institut für Anorganische Chemie, Karlsruher Institut für Technologie (KIT), Engesserstrasse 15, 76131 Karlsruhe, Germany

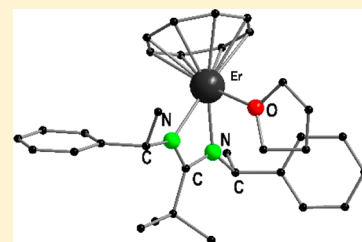
<sup>‡</sup>Department of Chemistry, Aarhus University, Langelandsgade 140, 8000 Aarhus C, Denmark

<sup>§</sup>Institut für Nanotechnologie, Karlsruher Institut für Technologie (KIT), Postfach 3640, 76021 Karlsruhe, Germany

<sup>||</sup>Institut de Physique et Chimie des Matériaux de Strasbourg (IPCMS), CNRS-Université de Strasbourg, 23 rue du Loess, BP 43, Strasbourg CEDEX 2 F-67034, France

## Supporting Information

**ABSTRACT:** Novel chiral rare-earth half sandwich complexes containing the chiral amidinate ligand, (*S,S*)-*N,N'*-bis(1-phenylethyl)benzamidinate ((*S*)-PEBA) or the *t*Bu analogue (*S,S*)-*N,N'*-bis(1-phenylethyl) pivalamidinate ((*S*)-PETA) and the cyclooctatetraene dianion (C<sub>8</sub>H<sub>8</sub>)<sup>2-</sup> (COT) were synthesized. All complexes were fully characterized and the solid state structures were established by single-crystal crystallography. Magnetic property measurements indicated that the complex [(*S*)-PETA]Er(COT)(THF)] is a typical field-induced single-molecule magnet (SMM), of which the magnetic properties are in reasonable agreement with high-level quantum chemical calculations. Due to predominantly electrostatic ligand field effects, the relativistic *J* = 15/2 ground manifold of Er(III) is split into 8 Kramers doublets spanning a range of ~500 cm<sup>-1</sup>, representable by means of higher order spin tensor operators. According to the quantum chemical calculations as well as from analysis of the experimental data, the magnetic relaxation pathways in these complexes are most likely to be of vibrational rather than electronic origin.



## INTRODUCTION

Along with the widely established cyclopentadienyl ligand and its derivatives, the cyclooctatetraene dianion (C<sub>8</sub>H<sub>8</sub>)<sup>2-</sup> (COT) is one of the most important ligands in organo-f-element chemistry.<sup>1–3</sup> The large and flat cyclooctatetraene ligand represents a valuable alternative to the cyclopentadienyl ligands.<sup>4,5</sup> Pioneering work on cyclooctatetraene lanthanide organometallic chemistry was reported by Streitwieser and co-workers in 1970.<sup>6</sup> Since then, numerous lanthanide cyclooctatetraene complexes with different structural motifs have been published.<sup>1–3</sup> Among the longest known lanthanide COT complexes are symmetrical sandwich complexes containing [Ln(C<sub>8</sub>H<sub>8</sub>)<sub>2</sub>]<sup>-</sup> anions.<sup>7–9</sup> Also, triple-decker complexes with a COT middle deck [(μ-η<sup>8</sup>:η<sup>8</sup>-COT){Ln(η<sup>5</sup>-Cp\*)}<sub>2</sub>]<sup>10,11</sup> (Cp\* = η<sup>5</sup>-C<sub>5</sub>Me<sub>5</sub>) have been reported for a series of divalent lanthanides. Spectacular structures were obtained by using silyl-substituted COT ligands such as [C<sub>8</sub>H<sub>6</sub>(SiMe<sub>3</sub>)<sub>2</sub>-1,4]<sup>2-</sup> (= COT''),<sup>12</sup> [C<sub>8</sub>H<sub>6</sub>(Si<sup>i</sup>Pr<sub>3</sub>)<sub>2</sub>-1,4]<sup>2-</sup> (= COT<sup>1,4Si<sup>i</sup>Pr<sub>3</sub></sup>),<sup>13</sup> and [1,4-R<sub>2</sub>C<sub>8</sub>H<sub>6</sub>]<sup>2-</sup> (R = *o*-(dimethylsilyl)-*N,N*-dimethylaniline).<sup>8,14</sup> These bulky COT ligands allowed for the synthesis of new double-decker and triple-decker sandwich-complexes, e.g., [(μ-η<sup>8</sup>:η<sup>8</sup>-COT<sup>1,4Si<sup>i</sup>Pr<sub>3</sub></sup>){LnCp\*}<sub>2</sub>]<sup>13</sup> and [(COT'')Ln(μ-η<sup>8</sup>:η<sup>8</sup>-COT'')Ln(COT'')] (Ln = Ce, Nd, Sm).<sup>12</sup> Besides these examples, numerous half-sandwich complexes [Ln(COT)R] (R = monoanionic ligand) such as R = Cl,<sup>6</sup> I,<sup>15,16</sup> O<sub>3</sub>SCF<sub>3</sub>,<sup>15</sup>

OR,<sup>17</sup> SR,<sup>18</sup> BH<sub>4</sub>,<sup>19</sup> (Ph<sub>2</sub>P)<sub>2</sub>N,<sup>20</sup> aminotroponimines,<sup>5</sup> 1,4-diazadienes,<sup>21</sup> and {CH(PPh<sub>2</sub>NSiMe<sub>3</sub>)<sub>2</sub>}<sup>22,23</sup> have been synthesized.

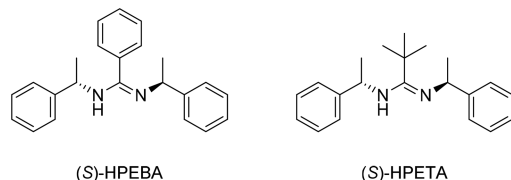
Lanthanide cyclooctatetraene complexes have also been used as catalysts for hydroamination reactions,<sup>22,23</sup> but the most recent application is the use as single-ion magnets (SIMs).<sup>24,25</sup> In 2011, Murugesu et al. reported the Dy sandwich complex, [Dy(COT'')<sub>2</sub>Li(THF)(DME)], which showed single-molecule magnet (SMM) behavior and unusual multiple relaxation modes.<sup>26</sup> Gao et al. synthesized the heteroleptic lanthanide complex [ErCp\*(COT)], which displayed a butterfly-shaped hysteresis loop at 1.8 K persisting up to 5 K.<sup>27</sup> After that, several novel lanthanide COT and COT'' single ion complexes have been investigated in terms of their SIM behavior.<sup>28–32</sup> As pointed out by Gao et al., the local symmetry generated by the ligand-field plays a crucial role for the design of SIMs.<sup>27,33–38</sup> The most spectacular advances in this area were reported recently by using rare-earth metal compounds, e.g., as shown last year when a Dy(III) metallocene exhibits a record high anisotropy barrier.<sup>39,40</sup> Since sandwich complexes possessing interesting magnetic properties,<sup>41</sup> we were interested to study the magnetic properties of a half-sandwich complex having a

Received: June 14, 2018

Published: October 17, 2018

second asymmetric ligand in the coordination sphere. Therefore, we synthesized a series of chiral lanthanide COT amidinate complexes. We employed two different chiral amidinate ligands, which were reported by us earlier in terms of catalytic applications.<sup>42–45</sup> These ligands are the chiral amidinate ((*S,S*)-*N,N'*-bis(1-phenylethyl) benzamidinate (*S*)-PEBA; Scheme 1)<sup>42–44,46</sup> and the <sup>t</sup>Bu analogue (*S,S*)-*N,N'*-bis(1-phenylethyl) pivalamidinate ((*S*)-PETA); Scheme 1).<sup>45</sup>

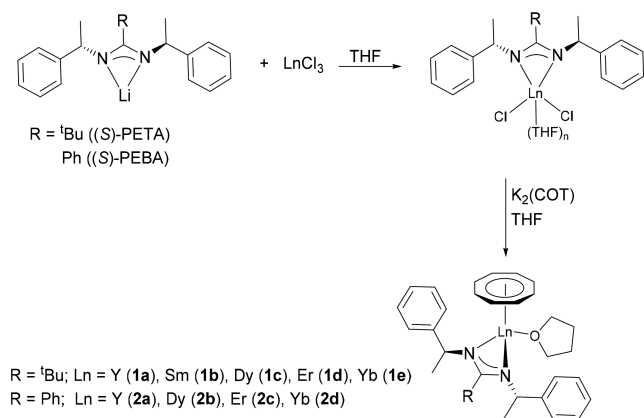
**Scheme 1.** Chiral Amidines (*S*)-HPEBA and (*S*)-HPETA



## DISCUSSION

**Synthesis.**<sup>47,48</sup> The title compounds [ $\{(S)\text{-PETA}\}\text{Ln}(\text{COT})(\text{THF})$ ] (Ln = Y (**1a**), Sm (**1b**), Dy (**1c**), Er (**1d**), and Yb (**1e**)) and [ $\{(S)\text{-PEBA}\}\text{Ln}(\text{COT})(\text{THF})$ ] (Ln = Y (**2a**), Dy (**2b**), Er (**2c**), and Yb (**2d**)), respectively, were synthesized by two-step reactions (Scheme 2). Anhydrous

**Scheme 2.** Synthesis of **1a–1e** and **2a–2d**



$\text{LnCl}_3$  salts were first reacted with Li(*S*)-PETA or Li(*S*)-PEBA in 1:1 stoichiometric ratio at room temperature to give [ $\text{Ln}((S)\text{-PETA})\text{Cl}_2(\text{THF})_n$ ]<sup>45</sup> or [ $\text{Ln}((S)\text{-PEBA})\text{Cl}_2(\text{THF})_n$ ]<sup>49</sup> *in situ*. Then, the resulting intermediates were mixed with freshly prepared  $\text{K}_2(\text{COT})$  and stirred for 24 h at room temperature. Crude products **1a–1e** and **2a–2d** were crystallized from *n*-pentane or *n*-pentane/toluene (Scheme 2). All complexes show the expected colors: Sm complex **1b**, red; Yb complexes **1e** and **2d**, green; Y complexes **1a** and **2a**, light yellow; Dy complexes **1c** and **2b**, yellow; Er complexes **1d** and **2c**, pink.

All compounds were characterized by IR spectroscopy and elemental analysis. NMR spectra were recorded only for diamagnetic compounds **1a** and **2a**. A strong peak at 1630–1590  $\text{cm}^{-1}$  assigned to the C–N vibration of the amidinate ligand, was observed in the IR spectra of all complexes. In the <sup>1</sup>H NMR spectra of **1a** and **2a**, a sharp singlet peak was observed at  $\delta$  6.71 (**1a**), 6.84 (**2a**) for the aromatic  $\eta^8$ -COT ring. These peaks are slightly shifted in comparison to the typical singlet peak of the COT ring, e.g., in [ $\{\text{CH-}$

( $\text{PPh}_2\text{NSiMe}_3\text{)}_2\text{Y}(\text{COT})$ ]<sup>22</sup>  $\delta$  6.54 ppm. In the NMR spectrum a symmetric coordination of the (*S*)-PEBA ligand is seen. The signal of the Ar–CHMe proton of the (*S*)-PETA ligand in **1a** is observed at  $\delta$  4.69 ppm, and the signal of the corresponding methyl group at  $\delta$  1.43 ppm. The Ar–CHMe proton of the (*S*)-PEBA ligand in **2a** appears as a quartet at  $\delta$  3.68 ppm and the signal of the corresponding methyl groups is seen at  $\delta$  1.24 ppm. In comparison to the corresponding peaks in K(*S*)-PEBA,<sup>46</sup> all peaks are upfield shifted by about 0.5 ppm in the NMR spectrum. Further details of the complex structures were deduced from the 2D <sup>1</sup>H, <sup>89</sup>Y gHMBC NMR spectra. The <sup>89</sup>Y signals at 68.3 ppm (**1a**) and 73.6 ppm (**2a**) in the NMR spectrum show cross peaks to the OCH<sub>2</sub> group of THF molecule and the COT ring.

Single crystals suitable for X-ray diffraction of all the compounds except **1a** were obtained by slowly evaporating a pentane solution. In contrast, single crystals of **1a** were grown by layering pentane on a toluene solution of the complex. All complexes are mononuclear and have similar structures, although they crystallize in two different space groups.

Crystallographic data for **1a–2d** are summarized in Tables S1 and S2. Compounds **1a,c,d** crystallize in the acentric orthorhombic space group  $P2_12_12_1$ . The molecular structure of **1a** is displayed as an example in Figure 1. In contrast,

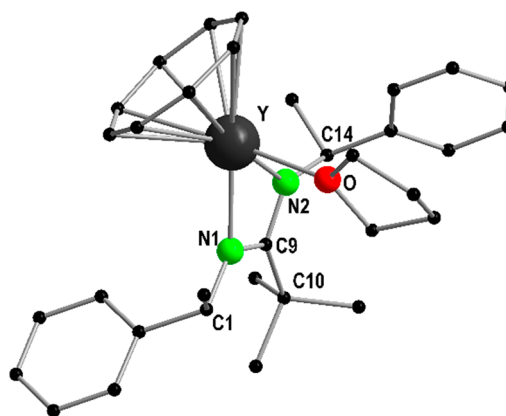


**Figure 1.** Molecular structure of **1a** in solid state, omitting the hydrogen atoms and solvent molecules. Selected bond lengths [Å] or angles [°]: (data for the compounds **1d,e** are also given). **1a**:  $\text{Cg}_{(\text{COT})}\text{-Y}$  1.8454(5),  $\text{Y-N1}$  2.333(5),  $\text{Y-N2}$  2.365(5),  $\text{Y-O}$  2.421(5);  $\text{Cg}_{(\text{COT})}\text{-Y-N1}$  139.7(2),  $\text{Cg}_{(\text{COT})}\text{-Y-N2}$  138.9(2),  $\text{N1-Y-N2}$  55.9(2),  $\text{N1-C9-N2}$  111.1(5). **1d**:  $\text{Cg}_{(\text{COT})}\text{-Er}$  1.8285(3),  $\text{Er-N1}$  2.315(4),  $\text{Er-N2}$  2.353(3),  $\text{Er-O}$  2.399(3);  $\text{Cg}_{(\text{COT})}\text{-Er-N1}$  139.51(15),  $\text{Cg}_{(\text{COT})}\text{-Er-N2}$  138.80(15),  $\text{N1-Er-N2}$  56.20(12),  $\text{N1-C9-N2}$  110.9(3). **1e**:  $\text{Cg}_{(\text{COT})}\text{-Yb}$  1.8033(3),  $\text{Yb-N1}$  2.323(5),  $\text{Yb-N2}$  2.315(6),  $\text{Yb-O}$  2.367(5);  $\text{Cg}_{(\text{COT})}\text{-Yb-N1}$  141.23(2),  $\text{Cg}_{(\text{COT})}\text{-Yb-N2}$  134.83(3),  $\text{N1-Yb-N2}$  56.80(2),  $\text{N1-C9-N2}$  110.0(5). Cg = ring centroid. Although, compounds **1b,c** are crystallizing in another space group, the corresponding bonding parameters are given here for comparison: **1b**:  $\text{Cg}_{(\text{COT})}\text{-Sm1}$  1.9487(8),  $\text{Sm1-N1}$  2.425(5),  $\text{Sm1-N2}$  2.447(5),  $\text{Sm1-O1}$  2.484(4),  $\text{Cg}_{(\text{COT})}\text{-Sm2}$  1.9337(4),  $\text{Sm2-N3}$  2.411(5),  $\text{Sm2-N4}$  2.443(5),  $\text{Sm2-O2}$  2.506(4);  $\text{Cg}_{(\text{COT})}\text{-Sm1-N1}$  144.4(2),  $\text{Cg}_{(\text{COT})}\text{-Sm1-N2}$  134.18(15),  $\text{N1-Sm1-N2}$  53.30(15),  $\text{N1-C9-N2}$  108.8(5),  $\text{N3-Sm2-N4}$  53.77(16),  $\text{N3-C42-N4}$  109.9(5). **1c**:  $\text{Cg}_{(\text{COT})}\text{-Dy1}$  1.8568(4),  $\text{Dy1-N1}$  2.358(8),  $\text{Dy1-N2}$  2.397(8),  $\text{Dy1-O1}$  2.419(6),  $\text{Cg}_{(\text{COT})}\text{-Dy2}$  1.8596(7),  $\text{Dy2-N3}$  2.344(7),  $\text{Dy2-N4}$  2.381(8),  $\text{Dy2-O2}$  2.456(7);  $\text{Cg}_{(\text{COT})}\text{-Dy1-N1}$  140.515(1),  $\text{Cg}_{(\text{COT})}\text{-Dy1-N2}$  142.721(2),  $\text{N1-Dy1-N2}$  55.4(3),  $\text{N1-C9-N2}$  110.8(8),  $\text{N3-Dy2-N4}$  55.2(3),  $\text{N3-C42-N4}$  111.4(9).

compounds **1b** and **1e** crystallize in the monoclinic space group  $P2_1$ . For **1a**, there is one molecule of the corresponding complex and one molecule of toluene in the asymmetric unit **1a** (Figure 1). In contrast, there are two lanthanide molecules with one molecule of solvent in the asymmetric unit of **1b** or **1c**. For **1d** and **1e**, again only one molecule of the corresponding complex is seen in the asymmetric unit. In all complexes, the rare-earth ion is coordinated by two N atoms from the (*S*)-PETA ligand, one O atom from THF, and the eight carbon atoms of the aromatic  $\eta^8$ -COT ring. Thus, a three-legged piano stool conformation is formed. The bond distances and angles are in the expected range. Thus, the average Ln–C(<sub>COT</sub>) length is 2.584(8) Å (**1a**), 2.673(6) Å (**1b**), 2.588(13) Å (**1c**), 2.571(6) Å (**1d**), and 2.565(8) Å (**1e**), while the distance of Ln to the centroid of the COT ring (Cg(<sub>COT</sub>)) is 1.8454(5) Å (**1a**), 1.9407(5) Å (**1b**), 1.8582(5) Å (**1c**), 1.8285(3) Å (**1d**), and 1.8033(3) Å (**1e**). Both values are comparable to those reported in the literature, e.g., for [K(18-c-6)(THF)<sub>2</sub>][Y(COT)<sub>2</sub>].<sup>50</sup>

Due to the crystal quality of **2a**, the collected diffraction data were not sufficient to solve the crystal structure. As it is difficult to get good quality crystal, for **2a** only the unit cell was determined. Compound **2c** is isostructural to (*S*)-PEBA complexes **2d** and **2e**. They crystallize in the acentric triclinic space group  $P1$ , each with two molecules of the complexes in the asymmetric unit. The differences in bond lengths and angles of all four compounds are a result of the lanthanide contraction.

As a representative example, the structure of **2c** is discussed in detail (Figure 2). In the solid-state structure, the expected  $\eta^8$

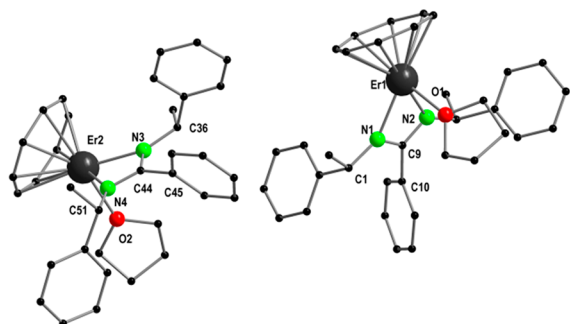


**Figure 2.** Molecular structure of **2c** in solid state, omitting the hydrogen atoms for clarity. Selected bond lengths [Å] or angles [°] (data for the isostructural compounds **2c** and **2d** are also given): **2c**: Cg(<sub>COT</sub>)1–Er1 1.8074(2), Er1–N1 2.338(5), Er1–N2 2.356(5), Er1–O1 2.376(4), Cg(<sub>COT</sub>)2–Er2 1.7948(2), Er2–N3 2.336(5), Er2–N4 2.342(5), Er2–O2 2.380(4); Cg(<sub>COT</sub>)1–Er1–N1 138.05(15), Cg(<sub>COT</sub>)1–Er1–N2 139.69(15), N1–Er1–N2 57.23(2), N1–C9–N2 115.6(5), N3–Er2–N4 57.43(2), N3–C44–N4 114.4(5). **2d**: Cg(<sub>COT</sub>)1–Yb1 1.7861(3), Yb1–N1 2.338(7), Yb1–N2 2.322(7), Yb1–O1 2.360(6), Cg(<sub>COT</sub>)2–Yb2 1.7690(3), Yb2–N3 2.319(7), Yb2–N4 2.310(7), Yb2–O2 2.364(6); Cg(<sub>COT</sub>)1–Yb1–N1 139.1(2), Cg(<sub>COT</sub>)1–Yb1–N2 137.5(2), N1–Yb1–N2 57.8(2), N1–C9–N2 115.5(7), N3–Yb2–N4 58.1(2), N3–C44–N4 115.8(7). Although compound **2b** crystallizes in another space group, the corresponding bonding parameters are given here for comparison: Cg(<sub>COT</sub>)–Dy 1.8443(3), Dy–N1 2.361(3), Dy–N2 2.401(3), Dy–O1 2.417(3); Cg(<sub>COT</sub>)–Dy–N1 137.01(10), Cg(<sub>COT</sub>)–Dy–N2 136.36(9), N1–Dy–N2 56.37(11), N1–C9–N2 115.4(3).

coordination of the COT ligand is seen. The planar  $\eta^8$ -ring shows no significant distortion within the carbon framework (average C–C bond distances 1.4074 Å). The Er–Cg(<sub>COT</sub>)

distances are in the range between 2.551(7) and 2.606(7) Å, with an average value of 2.574 Å, which is in agreement with [CH(PPh<sub>2</sub>NSiMe<sub>3</sub>)<sub>2</sub>ErCOT] (2.560(3)–2.608(3) Å, avg 2.579 Å).<sup>22</sup> The (*S*)-PEBA group is almost symmetrically attached to the metal center (Er1–N1 2.338(5), Er1–N2 2.356(5), Er2–N3 2.336(5), and Er2–N4 2.342(5)).

Dy complex **2b** crystallizes in the orthorhombic space group  $P2_12_12_1$ . There are four complex molecules in each unit cell. Its structure is similar to those of **2c** and **2d**. The Dy–Cg(<sub>COT</sub>) distance (1.8443(3) Å), which is longer than that in [Dy(COT)(Cp\*)] (1.6393(2) Å),<sup>51</sup> is slightly shorter than that of [K(18-C-6)][Dy(COT)<sub>2</sub>] (1.9092(3) Å).

**Magnetic Properties.** The magnetic properties of Dy and Er compounds **1c**, **2b,c**, and **1d** were measured on polycrystalline samples. As shown in Figure 3, the  $\chi T$  products at 300 K

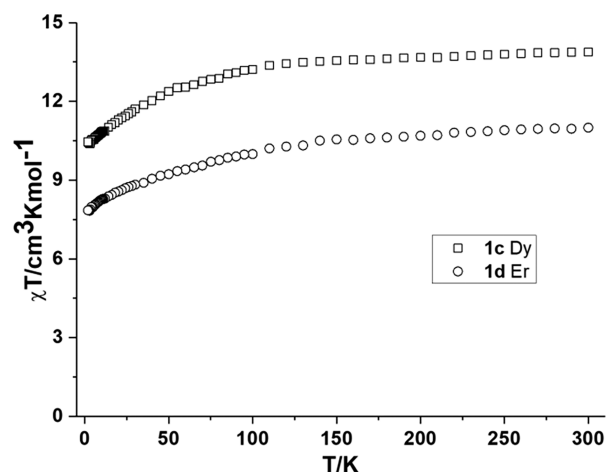


**Figure 3.** Plots of the  $\chi T$  vs  $T$  for complexes **1c**, Dy, and **1d**, Er, at 1000 Oe dc field.

of **1c** and **1d** are 13.88 and 11.00 cm<sup>3</sup> K mol<sup>-1</sup>, respectively, close to the expected value of 14.17 cm<sup>3</sup> K mol<sup>-1</sup> for one uncoupled Dy(III) metal ion ( $J = 15/2$ ,  $g = 4/3$ ) and 11.48 cm<sup>3</sup> K mol<sup>-1</sup> for one uncoupled Er(III) metal ion ( $J = 15/2$ ,  $g = 6/5$ ), respectively. Upon cooling, the  $\chi T$  products of both **1c** and **1d** decrease slowly from 300 to 100 K, then decrease more rapidly to reach 10.46 and 7.85 cm<sup>3</sup> K mol<sup>-1</sup> at 1.8 K, respectively. The continuous decrease of the  $\chi T$  product on lowering the temperature can be explained as result of the progressive depopulation of  $m_j$  sublevels and magnetic anisotropy of Dy(III) and Er(III) ions.<sup>50,52</sup> The corresponding magnetic data for compounds **2b** and **2c** are shown in Figure S30. The field dependence of magnetization of **1c** and **1d** from zero dc field to 7 T at 2, 3, and 5 K are shown in Figure 4, and the corresponding maximum values reached are 5.42 and 4.38  $\mu_B$ . The lack of saturation of magnetization at 7 T can likely be attributed to the inherent magnetic anisotropy of the metal ions.<sup>53–56</sup>

In order to verify their potential SMM behavior alternating current (ac) magnetic susceptibility studies were carried out on freshly filtered samples of **1c**, **1d**, **2b**, and **2c**. The magnetization relaxation of all systems was probed under zero dc field using ac susceptibility measurements as a function of the temperature at 1000 Hz. None of the complexes show an out-of-phase signal without the application of a dc field (Figure S25). One reason for this finding could be the very fast quantum tunneling of the magnetization (QTM) commonly

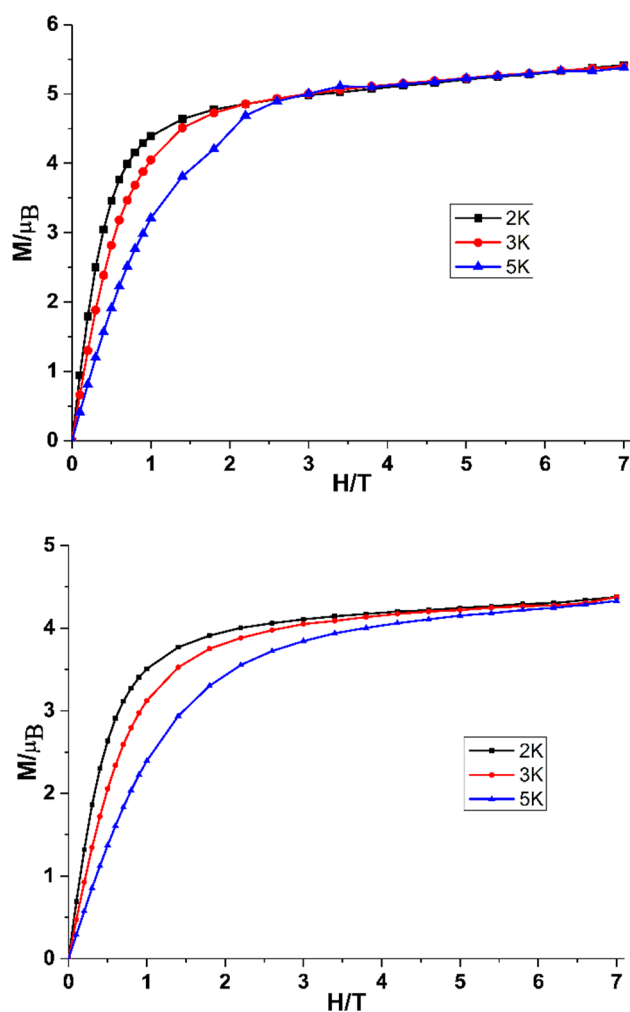


**Figure 4.** Plots of  $M$  vs  $H$  at 2, 3, and 5 K for complexes **1c**, Dy, (top), and **1d**, Er, (bottom). Lines are guides for the eye.

seen in pure lanthanide complexes.<sup>57,58</sup> In order to suppress QTM, ac susceptibility measurements in the presence of weak dc fields were performed (500–3000 Oe) at 1.8 K (Figure S26). For complexes **1c**, **2b**, and **2c**, no maximum in the out of phase ( $\chi''$ ) signal was observed even with an applied dc field indicating the absence of SMM behavior for these complexes, in contrast to **1d**, which exhibits slow relaxation of magnetization under applied static fields. The most effective suppression of QTM was observed at  $H_{dc} = 1000$  Oe. Therefore, ac susceptibility measurements for **1d** were carried out at this field strength (Figures 5, 6, and S27) revealing the typical behavior for a field-induced SMM. Cole–Cole plots of  $\chi'$  versus  $\chi''$ , between 2.8 and 7.2 K (Figure S28) revealed semicircular profiles and were fitted to a generalized Debye model with  $\alpha$  ranging from 0.01 to 0.12. This indicates a narrow distribution of relaxation processes in complex **1d**. To extract the associated relaxation parameters,<sup>59</sup> an Arrhenius plot of the relaxation time ( $\tau$ ) against  $1/T$  was constructed (Figure 7). The high temperature region was fitted to a straight line giving an Orbach energy barrier of 49.7 K and a relaxation time of  $1.8 \times 10^{-7}$  s. Owing to the significant deviation from linear behavior at low temperatures, the following eq 1 was used to analyze the relaxation data over the whole temperature range:

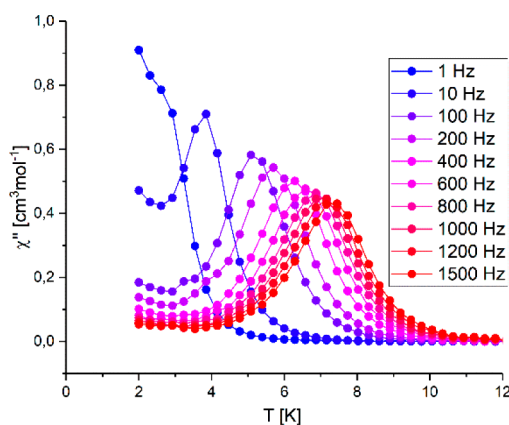


**Figure 5.** Plots  $\chi''$  vs temperature for complex **1d**, Er, with a dc field of 1000 Oe.

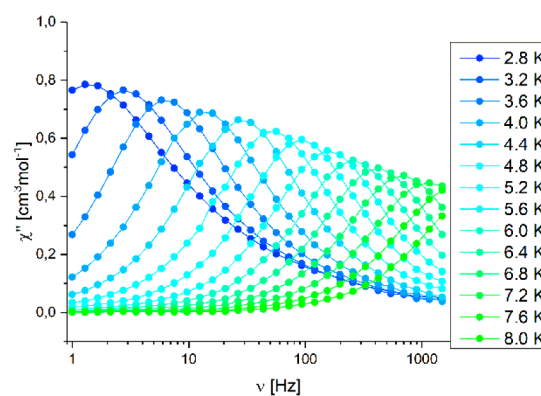


**Figure 6.** Plots  $\chi''$  vs frequency for complex **1d**, Er, with a dc field of 1000 Oe.

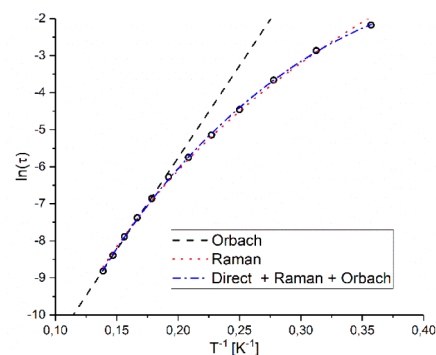


**Figure 7.** Plots of  $\ln(\tau)$  vs  $T^{-1}$  for **1d** under 1000 Oe dc field. Circles represent experimental data. The different lines represent different fits that were used to analyze the data.

$$\tau^{-1} = AT + B + CT^n + \tau_0^{-1} e^{-E_{\text{eff}}/k_B T} \quad (1)$$

The first two terms ( $AT$  and  $B$ ) describe the direct relaxation and QTM processes, the third term ( $CT^n$ ) describes a Raman process, and the fourth term ( $\tau_0^{-1} e^{-E_{\text{eff}}/k_B T}$ ) describes an Orbach process. The results of the fit are given in Table S12. Although the fit using eq 1 is slightly better, the complete Arrhenius diagram can be fitted using only the Raman term of eq 1 indicating that this is the dominant relaxation mechanism. Because of the constrained nature of metal– $\eta^8$ -COT vibrations,<sup>40</sup> we conjecture that a major relaxation pathway comprises the THF and (S)-PEBA ligands. Furthermore, it

cannot be excluded that electronic effects, like the reduced electron density of the N-ligands resulting from substituting the <sup>t</sup>Bu with a phenyl group or other ligand field effects could facilitate dissipation in **2b** and **2c**.

**Calculated Magnetic Data.** Quantum chemical calculations were performed to obtain zero-field splittings as well as macroscopic magnetic properties for Er(III) compounds **1d** and **2c**, as well as the Yb(III) **1e** and Dy(III) derivatives **1c** (see the “Quantum Chemical Calculations” section). The calculated magnetic susceptibilities and field-dependent magnetization show reasonable agreement with the experimental data (Figures 8 and S30, as well as Tables S4 and S5, respectively). The calculated values of the susceptibility of **1d** and **2c** are in the typical range for other Er(III) complexes.<sup>52</sup> Deviations between measured and calculated susceptibilities occur mainly in the low temperature range. Here, it has to be recognized that only isolated molecules are considered in the calculations.

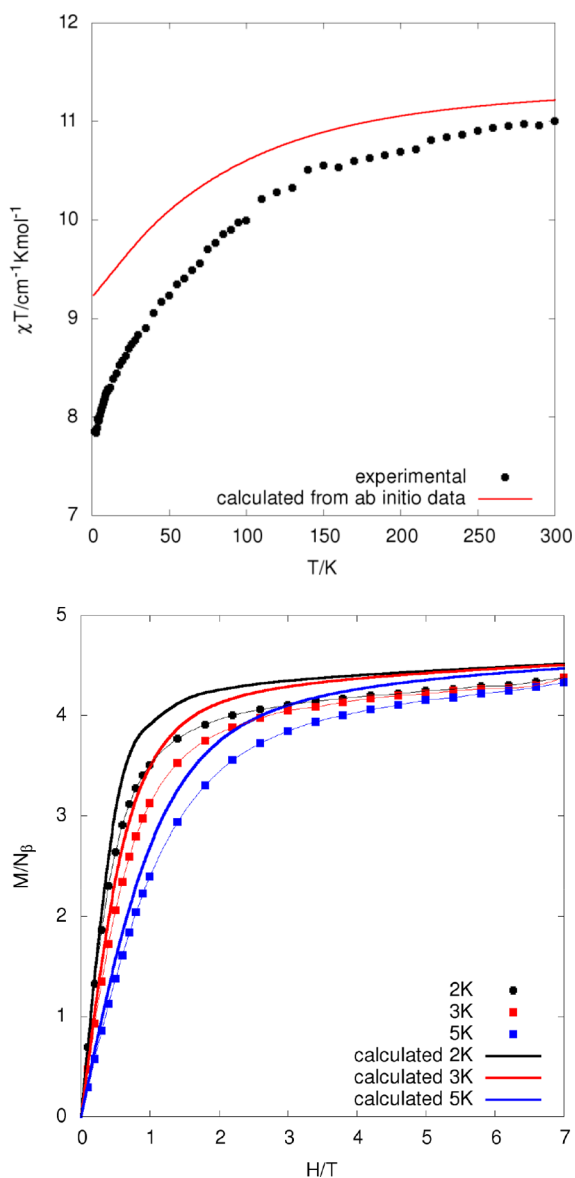


**Figure 8.** Comparison of the calculated and measured susceptibilities (top) and the field dependence of the magnetization at 2, 3, and 5 K for **1d**.

Considering the field-induced Er(III) based SMM, **1d**, the calculated magnetization is very similar to the experimental data for small fields and increases to slightly larger values for higher fields. The energy spectrum of the eight lowest Kramers doublets (Table 1) stemming from the <sup>4</sup>I<sub>15/2</sub> ground state of

**Table 1.** Energies (in cm<sup>-1</sup>) of the Lowest Electronic States of **1d** without and with Inclusion of Spin–Orbit Coupling<sup>a</sup>

	CASSCF/CI <sup>b</sup>	CASPT2 <sup>b</sup>	SOCI <sup>c</sup>	SOCI* <sup>c</sup>	
1	0 (0)	221 (119)	1	0 (0)	0
2	9 (12)	0 (0)	2	64 (50)	124
3	42 (37)	511 (231)	3	110 (102)	186
4	81 (75)	482 (302)	4	131 (130)	212
5	110 (109)	248 (219)	5	185 (187)	283
6	143 (147)	130 (198)	6	260 (271)	331
7	228 (237)	395 (353)	7	374 (390)	439
8	290 (306)	362 (371)	8	435 (459)	590
9	332 (351)	542 (476)			
10	391 (413)	581 (500)			
11	393 (415)	490 (477)			
12	497 (534)	811 (680)			
13	498 (534)	801 (680)			

<sup>a</sup>CAS(11,7)SCF/CI level and CAS(11,7)PT2 level; CAS(11,14) values in parentheses. <sup>b</sup>The CASSCF/CASPT2 states correspond to the <sup>4</sup>I term of the free ion in presence of the ligand field. <sup>c</sup>Spin–orbit coupling (SOCI and SOCI\*) within the full active space (only the first 32 microstates in the (11,14) case) results in eight low lying Kramers doublets which correspond to the *J* = 15/2 ground state of the <sup>4</sup>I. The next states follow at 6600 cm<sup>-1</sup>.

the free ion indicate a significant rhombicity induced by the asymmetric ligand field. This is in line with the experimental behavior, namely, the low value of the Orbach barrier compared to the energy of the first excited state and the fast relaxation observed for zero dc field. Owing to the asymmetry of the ligand field, the low energy spectrum is insufficiently described using the well-established second-order description involving the D-tensor. However, a reasonable agreement is achieved using higher (fourth to eighth) order (extended Stevens) operator equivalents (Table S6) comprising terms of lower symmetry, e.g., *S*<sub>2</sub>*S*<sub>4</sub>. Considering all eight Kramers doublets (*J* = 15/2) an isotropic *g*-tensor with *g* = 1.19 identical to the value of the free ion was obtained. For the first Kramers doublet and an effective spin of *S* = 1/2, an axial *g*-tensor with *g*<sub>z</sub> = 17.2 and *g*<sub>x</sub> and *g*<sub>y</sub> close to zero is observed. The values for the other low lying Kramers doublets are listed in Table S7.

The electronic and thus magnetic properties of the other Er(III) based complex **2c** are rather similar to those obtained for **1d** (see Tables S7 and S8 and Figure S30). However, since **2c** does not show slow magnetic relaxation, we conjecture that vibrational rather than electronic effects dominate magnetic relaxation in **1d**.

The magnetic structures of the non-SMM complexes based on Yb(III) and Dy(III) do not display distinct axial behavior (Table S10). As in **1d**, relaxation via electronically excited states is not the dominant channel for both **1c** and **1e** because of the magnitude of the first excitation energy (82 cm<sup>-1</sup> for **1c**, 334 cm<sup>-1</sup> for **1e**).

Thus, based on the results of our quantum chemical calculations, a fast relaxation via spin–phonon coupling is

more likely than Orbach-type processes, although other effects facilitating quantum tunneling effects cannot be excluded.

## CONCLUSION

A series of chiral lanthanide complexes based on (S)-PEBA/(S)-PETA and COT has been synthesized and the compounds fully characterized. A study of the magnetic properties of Dy and Er compounds **1c** and **1d** indicated that complex **1d** is a typical field-induced SIM. Quantum chemical calculations on the electronic states corresponding to the  $^4I_{15/2}$  ground term states reveal the presence of an axial *g*-tensor for the lowest Kramers doublet. For the quantitative description of the ligand field splitting, higher order Stevens operators are necessary in order to account for the inherent ligand field asymmetry. Due to the temperature dependence of the magnetic relaxation data, and supported by quantum chemical calculations, Raman-type relaxation mechanisms are suggested to play a dominant role in the asymmetric lanthanide complexes investigated.

## EXPERIMENTAL SECTION

**General Methods.** All air- and water-sensitive materials were prepared under nitrogen atmosphere by using either Schlenk line or glovebox. THF was dried by distilling from potassium benzophenone ketyl under nitrogen before use. Toluene and *n*-pentane were dried with a MBraun solvent purification system (SPS-800). Deuterated solvents were purchased from Carl Roth GmbH (99.5 atom % D) and were dried and stored under vacuum with Na/K alloy. NMR spectra were recorded on a Bruker Avance II 300 MHz or Bruker Avance III 400 MHz. Chemical shifts are referenced to internal solvent resonances and are reported relative to tetramethylsilane ( $^1\text{H}$  and  $^{13}\text{C}$  NMR) and  $[\text{Y}(\text{NO}_3)_3]$  ( $^{89}\text{Y}$  NMR), respectively. Elemental analyses were carried out with an Elementar Vario Micro Cube. IR spectra were performed on a Bruker TENSOR 37 spectrometer via the attenuated total reflection method (ATR).  $\text{LnCl}_3$ ,<sup>60</sup> lithium-*N,N'*-bis((S)-1-phenylethyl)benzamidinate (Li(S)-PEBA),<sup>46,61</sup> lithium-*N,N'*-bis((S)-1-phenylethyl)*tert*-butylamidinate (Li(S)-PETA),<sup>61</sup> and  $\text{K}_2\text{C}_8\text{H}_8$  ( $\text{K}_2\text{COT}$ )<sup>62</sup> were prepared following the literature procedures. The other chemicals were commercially available and used without further purification.

Magnetic susceptibility data (1.8–300K) were collected on powdered samples using a Quantum Design model MPMS-XL SQUID instrument under a 1000 Oe applied magnetic field. Magnetization isotherms were collected at 2, 3 and 5 K between 0 and 7T. The ac susceptibility measurements were carried out under an oscillating ac field of 3 Oe and ac frequencies ranging from 1 to 1500 Hz. Data were corrected for diamagnetism using Pascal constants and a sample holder correction.

**Synthesis of  $[\{(S)\text{-PETA}\}_n\text{Ln}(\text{COT})(\text{THF})]$  [ $\text{Ln} = \text{Y}(\mathbf{1a}), \text{Sm}(\mathbf{1b}), \text{Dy}(\mathbf{1c}), \text{Er}(\mathbf{1d}), \text{Yb}(\mathbf{1e})$ ].<sup>48</sup>** Anhydrous  $\text{LnCl}_3$  (0.63 mmol) was treated with Li(S)-PETA (200 mg, 0.63 mmol) in 10 mL of THF under a nitrogen atmosphere. The reaction was allowed to warm up to room temperature and kept stirring for 1 h. Then, 10 mL of THF solution of freshly prepared  $\text{K}_2\text{COT}$  was added, and immediately, a color change was observed. After stirring for an additional 24 h. THF was removed in vacuo, and 20 mL of *n*-pentane was added. The solid was removed by filtration and filtrate was concentrated. The residue was purified by crystallization from either *n*-pentane or toluene/*n*-pentane (1:2) (**1b**).

**1a.** Yellow crystals. Yield: 142 mg (based on single crystals), 0.248 mmol, 39%.  $^1\text{H}$  NMR (400.13 MHz,  $\text{C}_6\text{D}_6$ , 298 K):  $\delta$  (ppm) = 7.38 (d, *J* = 7.2 Hz, 4H, Ph), 7.25 (t, *J* = 7.6 Hz, 4H, Ph), 7.15–7.10 (m, 2H), 6.71 (s, 8H, COT), 4.69 (q, *J* = 5.8 Hz, 2H, CH), 3.24–3.14 (m, 2H,  $\text{CH}_2(\text{THF})$ ), 3.07–3.02 (m, 2H,  $\text{CH}_2(\text{THF})$ ), 1.42 (d, *J* = 5.8 Hz, 6H,  $\text{CH}_3$ ), 0.95 (s, 9H,  $\text{CH}_3$ ), 0.93–0.86 (m, 4H,  $\text{CH}_2(\text{THF})$ ).  $^{13}\text{C}\{^1\text{H}\}$  NMR (100.6 MHz,  $\text{C}_6\text{D}_6$ , 298 K):  $\delta$  (ppm) = 178.4 (NCN), 148.9 (*i*-Ph), 128.2 (Ph), 126.3 (Ph), 126.1 (Ph), 94.2 (COT), 69.7 ( $\text{CH}_2(\text{THF})$ ), 55.4 (CH), 28.8 (CCH<sub>3</sub>), 25.8 (NCHCH<sub>3</sub>), 24.7

( $\text{CH}_2(\text{THF})$ ), 23.0 ( $\text{C}(\text{CH}_3)_3$ ).  $^{89}\text{Y}\{^1\text{H}\}$  NMR (19.61 MHz,  $\text{C}_6\text{D}_6$ ):  $\delta$  (ppm) = 73.6. Anal. Calcd (%) for  $\text{C}_{33}\text{H}_{43}\text{YN}_2\text{O}$  (572.62): C, 69.22; H, 7.57; N, 4.89. Found: C, 69.86; H, 7.29; N, 4.42. IR (ATR)  $\nu/\text{cm}^{-1}$ : 2953 (s), 2922 (s), 1653 (s), 1635 (s), 1490 (s), 1476 (s), 1447 (s), 1065 (m), 1026 (m), 897 (w), 757 (s), 698  $\text{cm}^{-1}$  (vs).

**1b.** Red crystals. Yield: 132 mg (based on single crystals), 0.208 mmol, 33%. Anal. Calcd (%) for  $\text{C}_{33}\text{H}_{43}\text{SmN}_2\text{O}$  (634.07): C, 62.51; H, 6.84; N, 4.42. Found: C, 62.28; H, 6.71; N, 4.28. IR (ATR)  $\nu/\text{cm}^{-1}$ : 2961 (s), 2923 (s), 1633 (s), 1490 (s), 1476 (s), 1448 (s), 1364 (m), 1253 (m), 1190 (m), 1066 (m), 1020 (m), 756 (s), 697 (vs), 542  $\text{cm}^{-1}$  (s).

**1c.** Yellow crystals. Yield: 171 mg (based on single crystals), 0.265 mmol, 42%. Anal. Calcd (%) for  $\text{C}_{66}\text{H}_{86}\text{Dy}_2\text{N}_4\text{O}_2$  (1292.39): C, 61.34; H, 6.71; N, 4.34. Found: C, 61.07; H, 6.45; N, 4.20. IR (ATR)  $\nu/\text{cm}^{-1}$ : 2961 (s), 2923 (s), 2856 (s), 1602 (s), 1476 (s), 1448 (s), 1397 (s), 1364 (m), 1278 (m), 1191 (m), 1066 (m), 1025 (m), 938 (w), 750 (s), 698 (vs), 636 (w), 510  $\text{cm}^{-1}$  (s).

**1d.** Pink crystals. Yield: 111 mg (based on single crystals), 0.17 mmol, 27%. Anal. Calcd (%) for  $\text{C}_{29}\text{H}_{35}\text{ErN}_2$  (578.87) (= **1d** – THF): C, 60.17; H, 6.09; N, 4.84. Found: C, 60.09; H, 6.60; N, 4.43. IR (ATR)  $\nu/\text{cm}^{-1}$ : 2963 (s), 1653 (s), 1635 (s), 1490 (s), 1447 (m), 1400 (m), 1362 (m), 1299 (m), 1186 (m), 1149 (m), 1065 (m), 1027 (s), 865 (m), 758 (s), 698 (vs), 672  $\text{cm}^{-1}$  (s).

**1e.** Green crystals. Yield: 96 mg (based on single crystals), 0.146 mmol, 23%. Anal. Calcd (%) for  $\text{C}_{33}\text{H}_{43}\text{YbN}_2\text{O}$  (656.73): C, 60.35; H, 6.60; N, 4.27. Found: C, 60.01; H, 6.395; N, 4.14. IR (ATR)  $\nu/\text{cm}^{-1}$ : 2963 (s), 2923 (s), 1653 (s), 1633 (s), 1559 (w), 1541 (w), 1490 (s), 1476 (s), 1448 (s), 1191 (m), 1066 (m), 1025 (m), 756 (s), 698 (vs), 543  $\text{cm}^{-1}$  (s).

**Synthesis of  $[\{(S)\text{-PEBA}\}_n\text{Ln}(\text{COT})(\text{THF})]$  [ $\text{Ln} = \text{Y}(\mathbf{2a}), \text{Dy}(\mathbf{2b}), \text{Er}(\mathbf{2c}), \text{Yb}(\mathbf{2d})$ ].<sup>47</sup>** The synthesis of  $[\{(S)\text{-PEBA}\}_n\text{Ln}(\text{COT})(\text{THF})]$  was carried out following the similar method as that for  $[\{(S)\text{-PETA}\}_n\text{Ln}(\text{COT})(\text{THF})]$ .

**2a.** Yellow crystals. Yield: 88 mg (based on single crystals), 0.148 mmol, 25%.  $^1\text{H}$  NMR (400.13 MHz,  $\text{C}_6\text{D}_6$ , 298 K):  $\delta$  (ppm) = 7.14 (d, 6H, Ph), 7.11–7.01 (m, 4H, Ph), 6.92–6.90 (m, 3H, Ph), 6.83 (s, 8H, COT), 6.54–6.51 (m, 2H, Ph), 3.68 (m, *J* = 6.7 Hz, 1.7 Hz, 2H, CH), 3.10–3.03 (m, 4H, CH<sub>2</sub>(THF)), 1.23 (d, *J* = 6.7 Hz, 6H, CH<sub>3</sub>), 1.00–0.96 (m, 4H,  $\text{CH}_2(\text{THF})$ ).  $^{13}\text{C}\{^1\text{H}\}$  NMR (100.6 MHz,  $\text{C}_6\text{D}_6$ , 298 K):  $\delta$  (ppm) = 177.3 (NCN), 148.4 (*i*-Ph), 134.7 (*i*-Ph), 128.2 (Ph), 127.8 (Ph), 127.5 (Ph), 126.5 (Ph), 126.2 (Ph), 126.0 (Ph), 94.3 (COT), 69.8 ( $\text{CH}_2(\text{THF})$ ), 56.2 (CH), 25.1 (CH<sub>3</sub>), 24.9 ( $\text{CH}_2(\text{THF})$ ).  $^{89}\text{Y}\{^1\text{H}\}$  NMR (19.61 MHz,  $\text{C}_6\text{D}_6$ ):  $\delta$  (ppm) = 68.3. Anal. Calcd (%) for  $\text{C}_{35}\text{H}_{39}\text{YN}_2\text{O}$  (591.58): C, 70.94; H, 6.63; N, 4.73. Found: C, 70.25; H, 6.64; N, 4.67. IR (ATR)  $\nu/\text{cm}^{-1}$ : 3407 (m), 2955 (w), 2919 (w), 1637 (s), 1483 (s), 1451 (s), 1413 (s), 1309 (w), 1142 (m), 1072 (m), 1021 (m), 759 (s), 695 (vs), 541  $\text{cm}^{-1}$  (s).

**2b.** Yellow crystals. Yield: 86 mg (based on single crystals), 0.129 mmol, 22%. Anal. Calcd (%) for  $\text{C}_{35}\text{H}_{39}\text{DyN}_2\text{O}$  (666.18): C, 63.10; H, 5.90; N, 4.20. Found: C, 62.67; H, 5.98; N, 4.00. IR (ATR)  $\nu/\text{cm}^{-1}$ : 3300 (m), 2919 (w), 1700 (s), 1443 (s), 1373 (s), 1309 (w), 1298 (m), 1143 (m), 1072 (m), 1008 (m), 765 (s), 679 (vs), 477  $\text{cm}^{-1}$  (s).

**2c.** Pink crystals. Yield: 115 mg (based on single crystals), 0.171 mmol, 29%. Anal. Calcd (%) for  $\text{C}_{35}\text{H}_{39}\text{ErN}_2\text{O}$  (670.94): C, 62.65; H, 5.86; N, 4.18. Found: C, 63.07; H, 6.09; N, 4.17. IR (ATR)  $\nu/\text{cm}^{-1}$ : 3407 (w), 2955 (w), 2920 (w), 1637 (s), 1483 (s), 1446 (s), 1414 (s), 1365 (w), 1308 (w), 1268 (w), 1143 (w), 1072 (w), 1022 (m), 759 (s), 736 (m), 695 (vs), 601 (w), 573 (w), 541  $\text{cm}^{-1}$  (s).

**2d.** Green crystals. Yield: 129 mg (based on single crystals), 0.191 mmol, 32%. Anal. Calcd (%) for  $\text{C}_{31}\text{H}_{31}\text{YbN}_2$  (604.64) (= **2d** – THF): C, 61.58; H, 5.17; N, 4.63. Found: C, 61.00; H, 5.69; N, 3.92. IR (ATR)  $\nu/\text{cm}^{-1}$ : 3407 (m), 2955 (w), 2919 (w), 1636 (vs), 1482 (s), 1451 (s), 1309 (w), 1298 (w), 1268 (w), 1142 (m), 1072 (m), 1028 (m), 765 (s), 698 (vs), 601 (s), 572 (s), 546  $\text{cm}^{-1}$  (s).

**X-ray Crystallographic Studies of **1a–1e** and **2a–2d**.** A suitable crystal was covered in mineral oil (Aldrich) and mounted on

a glass fiber. The crystal was transferred directly to a cold stream of a STOE IPDS 2 or STOE StadiVari diffractometer.

All structures were solved by using the program SHELXS/T<sup>63,64</sup> using Olex2.<sup>65</sup> The remaining non-hydrogen atoms were located from successive difference Fourier map calculations. The refinements were carried out by using full-matrix least-squares techniques on  $F^2$  by using the program SHELXL.<sup>63,64</sup> In each case, the locations of the largest peaks in the final difference Fourier map calculations, as well as the magnitude of the residual electron densities, were of no chemical significance. Positional parameters, hydrogen atom parameters, thermal parameters, and bond distances and angles have been deposited in the [Supporting Information](#).

Data collection parameters are given in [Table S1](#). Crystallographic data (excluding structure factors) for the structures reported in this paper have been deposited with the Cambridge Crystallographic Data Centre and the relevant codes are 1847599–1847607. Copies of the data can be obtained free of charge on application to CCDC, 12 Union Road, Cambridge CB21EZ, UK (fax: +(44)1223–336–033; email: [deposit@ccdc.cam.ac.uk](mailto:deposit@ccdc.cam.ac.uk)).

**Quantum Chemical Calculations.**<sup>47</sup> For complexes **1c–e** and **2c**, quantum chemical calculations were performed to obtain the low energy states and the magnetic properties. All calculations are based on the experimental X-ray structure and were performed with the MOLCAS<sup>66</sup> and DIRAC<sup>67</sup> program packages if not mentioned elsewhere. In the MOLCAS calculations, an ANO-RCC basis<sup>68–70</sup> of triple- $\zeta$  quality was used for Dy, Yb, Er, N, and O, and a basis of double- $\zeta$  quality for C and H, the DIRAC calculations were performed on an Er embedded by a point charge model for the ligand field (see below) employing a dyall.v2z basis.<sup>71</sup>

Scalar relativistic effects were considered by the X2C operator.<sup>72</sup> Because of the open shell character of the Ln(III) ions, wave-function-based, multireference methods were applied: Energies and wave functions of the electronic states were therefore obtained by the nonrelativistic complete active space self-consistent field (CASSCF)<sup>73</sup> as well as the two-component relativistic Kramers-restricted complete active space configuration interaction method (KR-CASCI).<sup>74</sup>

In the CASSCF calculations, the active space contained the seven 4f orbitals of Ln occupied with 9, 11, and 13 electrons. The orbitals were optimized for an averaged density constructed from all high spin states (21 sextets for CAS(9,11), 35 quartets for CAS(11,7), 7 doublets in CAS(13,7)) with equal weighting factors. The energies of the low spin states were obtained in a CASCI (CI: configuration interaction) calculation within the same active space. For **1d**, dynamic correlation energies for the ground manifold were obtained by state-specific complete active space second-order perturbation theory (SS-CASPT2).<sup>75</sup> Spin orbit configuration interaction (SOC) was included using quasi degenerate perturbation theory by coupling all electronic states in the active space for **1d**, **1e**, and **2c** (147, 7, and 147 microstates). For **1c**, an energy cutoff of 10 eV was used (535 microstates).

The calculations were performed with the RASSI module of MOLCAS using an atomic mean field approximation (AMFI)<sup>76</sup> for the spin–orbit integrals. The results are based on CASSCF/CI wave functions. In the SOC calculations CASSCF/CI energies were taken, while in the SOC\* calculation for **1d**, the SS-CASPT2 energies are used for the 13 lowest states. All other states were shifted by the average of the correlation energies. The magnetic properties such as magnetic susceptibility and field dependent magnetization, as well as g-tensors of the lowest eight Kramers doublets with a pseudospin of 1/2 and zero-field splitting parameters for a pseudospin of 7/2 (Yb(III)) and 15/2 (Er(III), Dy(III)) were obtained with the Single-ANISO module.<sup>77,78</sup>

In order to check the influence of covalency of the ligands on the electronic structure of **1d**, calculations on an electrostatic model were additionally performed where the electric field was constructed from point charges located at the positions of the atoms in the full complex. The values of the point charges were obtained from a Mulliken analysis<sup>79</sup> of the CAS(11,7)SCF ground states. The splitting of the low energy states is only slightly changed and the g-tensor of the lowest state remains axial (see the [Supporting Information](#)).

Concerning the complexity of the nonrelativistic electronic structure, in particular the encountered root-flipping in the CASPT2 calculations on **1d**, the active space was enlarged by a second set of f-orbitals (CAS(11,14)SCF) in order to increase the flexibility of the reference wave functions and therefore improve the many-body perturbation theory treatment. The results are similar to the CAS(11,7) results confirming the root-flipping, but with a smaller separation of about 119  $\text{cm}^{-1}$ . The effects on the electronic states are shown in [Table 1](#) (values in parentheses). Because the effect of enlarging the active space on the electronic energies is considerably smaller than spin–orbit coupling, further calculations were dispensed. Instead, because of the importance of relativistic effects in lanthanide complex **1d**, the validity of the SOC approach was checked by means of two-component Kramers-restricted SCF and CI calculations using the DIRAC program suite (version 16).<sup>67</sup> In these calculations, spin–orbit effects are considered in all basis functions as well as in the orbital optimization procedure, yielding a relativistic benchmark for the quasi-relativistic CASSCF/SOCI approach. The KR-SCF and KR-CI calculations employ a Kramers-restricted 2-spinor basis with an X2C operator for one-electron integrals together with AMFI corrections for the two-electron contributions and were performed on a point charge model (for a detailed description of the procedure, see [Table S9](#)). These calculations confirm the findings obtained from the quasirelativistic CAS/SOCI calculations on similar point charge field models performed with the SOC program developed recently in Karlsruhe and Kaiserslautern ([Table S9](#)).<sup>47</sup> We therefore conclude that the chosen CAS( $n,7$ )SCF/PT2 // SOCI method ( $n = 9, 11, 13$ ) is adequate to describe the relativistic electronic and magnetic structure of the complexes under investigation.

## ■ ASSOCIATED CONTENT

### 📄 Supporting Information

The Supporting Information is available free of charge on the ACS Publications website at DOI: [10.1021/acs.organomet.8b00412](https://doi.org/10.1021/acs.organomet.8b00412).

Synthesis, IR, NMR, XRD, magnetic measurements, and quantum chemical calculations (PDF)

Cartesian coordinates (XYZ)

### Accession Codes

CCDC 1847599–1847607 contain the supplementary crystallographic data for this paper. These data can be obtained free of charge via [www.ccdc.cam.ac.uk/data\\_request/cif](http://www.ccdc.cam.ac.uk/data_request/cif), or by emailing [data\\_request@ccdc.cam.ac.uk](mailto:data_request@ccdc.cam.ac.uk), or by contacting The Cambridge Crystallographic Data Centre, 12 Union Road, Cambridge CB2 1EZ, UK; fax: +44 1223 336033.

## ■ AUTHOR INFORMATION

### Corresponding Authors

\*E-mail: [karin.fink@kit.edu](mailto:karin.fink@kit.edu) (K.F.).

\*E-mail: [annie.powell@kit.edu](mailto:annie.powell@kit.edu) (A.K.P.).

\*E-mail: [roesky@kit.edu](mailto:roesky@kit.edu) (P.W.R.).

### ORCID

Eufemio Moreno-Pineda: 0000-0002-9643-0341

Annie K. Powell: 0000-0003-3944-7427

Peter W. Roesky: 0000-0002-0915-3893

### Funding

This work was supported by the DFG-funded transregional collaborative research center SFB/TRR 88 “3MET”, projects A1, A3, B3, and C5. M.H. gratefully acknowledges a grant from the China Scholarship Council (No. 201206250015). T.B. and A.N. thank the Danish Council for Independent Research (DFR) for funding via FNU.

### Notes

The authors declare no competing financial interest.

## REFERENCES

- (1) Edlmann, F. T. Rare earth cyclooctatetraene complexes. Organolanthanide chemistry in three oxidation states. *New J. Chem.* **1995**, *19*, 535–550.
- (2) Edlmann, F. T. Scandium, Yttrium, Lanthanides and Actinides and Titanium, Zirconium and Hafnium. *Comprehensive Organometallic Chemistry II* **1995**, *4*, 11–212.
- (3) Edlmann, F. T. Cyclopentadienyl-free organolanthanide chemistry. *Angew. Chem., Int. Ed. Engl.* **1995**, *34*, 2466–88.
- (4) Edlmann, F. T.; Freckmann, D. M. M.; Schumann, H. Synthesis and Structural Chemistry of Non-Cyclopentadienyl Organolanthanide Complexes. *Chem. Rev.* **2002**, *102*, 1851–1896.
- (5) Roesky, P. W. Cyclooctatetraene complexes of yttrium and the lanthanides with chiral and achiral aminotroponimines. *J. Organomet. Chem.* **2001**, *621*, 277–283.
- (6) Mares, F.; Hodgson, K. O.; Streitwieser, A. Monocyclooctatetraenyl-lanthanide chlorides, a new class of cyclooctatetraene complexes. *J. Organomet. Chem.* **1971**, *28*, C24–C26.
- (7) Mares, F.; Hodgson, K.; Streitwieser, A. Lanthanide complexes with cyclooctatetraene di-anion. *J. Organomet. Chem.* **1970**, *24*, C68–C70.
- (8) Wetzel, T. G.; Dehnen, S.; Roesky, P. W. A Multifunctional Substituted Cyclooctatetraene as a Ligand in Organosamarium Chemistry. *Organometallics* **1999**, *18*, 3835–3842.
- (9) Hodgson, K. O.; Raymond, K. N. Ion pair complex formed between bis(cyclooctatetraenyl)cerium(III) anion and an ether-coordinated potassium cation. Crystal and molecular structure of  $[\text{K}(\text{CH}_3\text{OCH}_2\text{CH}_2)_2\text{O}][\text{Ce}(\text{C}_8\text{H}_8)_2]$ . *Inorg. Chem.* **1972**, *11*, 3030–3035.
- (10) Evans, W. J.; Johnston, M. A.; Greci, M. A.; Ziller, J. W. Synthesis, Structure, and Reactivity of Unsolvated Triple-Decked Bent Metallocenes of Divalent Europium and Ytterbium. *Organometallics* **1999**, *18*, 1460–1464.
- (11) Evans, W. J.; Clark, R. D.; Ansari, M. A.; Ziller, J. W. Bent vs Linear Metallocenes Involving  $\text{C}_5\text{Me}_5$  vs  $\text{C}_8\text{H}_8$  Ligands: Synthesis, Structure, and Reactivity of the Triple-Decked  $(\text{C}_5\text{Me}_5)(\text{THF})_x\text{Sm}(\text{C}_8\text{H}_8)\text{Sm}(\text{THF})_x(\text{C}_5\text{Me}_5)$  ( $x = 0, 1$ ) Complexes Including a Formal Two-Electron Oxidative Addition to a Single Lanthanide Metal Center. *J. Am. Chem. Soc.* **1998**, *120*, 9555–9563.
- (12) Poremba, P.; Edlmann, F. T. Cyclooctatetraenyl complexes of the early transition metals and lanthanides: X.1 The first organometallic triple decker sandwich complexes of the lanthanides. *J. Organomet. Chem.* **1998**, *553*, 393–395.
- (13) Summerscales, O. T.; Jones, S. C.; Cloke, F. G. N.; Hitchcock, P. B. Anti-Bimetallic Complexes of Divalent Lanthanides with Silylated Pentalene and Cyclooctatetraenyl Bridging Ligands as Molecular Models for Lanthanide-Based Polymers. *Organometallics* **2009**, *28*, 5896–5908.
- (14) Wetzel, T. G.; Roesky, P. W. A Functionalized Cyclooctatetraene as Ligand in Organolanthanide Chemistry. *Organometallics* **1998**, *17*, 4009–4013.
- (15) Kilimann, U.; Schäfer, M.; Herbst-Irmer, R.; Edlmann, F. T. Cyclooctatetraenyl komplexe der frühen Übergangsmetalle und lanthanoiden. *J. Organomet. Chem.* **1994**, *469*, C10–C14.
- (16) Mashima, K.; Shibahara, T.; Nakayama, Y.; Nakamura, A. Mononuclear  $\eta^8$ -cyclooctatetraenyl(thiolato)samarium(III) complexes  $(\eta^8\text{-C}_8\text{H}_8)\text{Sm}(\text{SR})(\text{hmpa})_2$  ( $\text{R} = 2,4,6$ -triisopropylphenyl and 2-pyridyl; HMPA = hexamethylphosphoric triamide) derived from metallic samarium, diaryl disulfide, and 1,3,5,7-cyclooctatetraene in the presence of HMPA. *J. Organomet. Chem.* **1998**, *559*, 197–201.
- (17) Schumann, H.; Winterfeld, J.; Köhn, R. D.; Esser, L.; Dietrich, A.; Sun, J. Metallorganische Verbindungen der Lanthanoide, 73. Synthese und Struktur neuer Monocyclooctatetraenyl-Komplexe von Yttrium, Terbium und Lutetium. *Chem. Ber.* **1993**, *126*, 907–912.
- (18) Cendrowski-Guillaume, S. M.; Le Gland, G.; Nierlich, M.; Ephritikhine, M. Lanthanide Borohydrides as Precursors to Organometallic Compounds. Mono(cyclooctatetraenyl) Neodymium Complexes. *Organometallics* **2000**, *19*, 5654–5660.
- (19) Cendrowski-Guillaume, S. M.; Nierlich, M.; Lance, M.; Ephritikhine, M. First Chemical Transformations of Lanthanide Borohydride Compounds: Synthesis and Crystal Structures of  $[(\eta\text{-C}_8\text{H}_8)\text{Nd}(\text{BH}_4)(\text{THF})]_2$  and  $[(\eta\text{-C}_8\text{H}_8)\text{Nd}(\text{THF})_4][\text{BPh}_4]$ . *Organometallics* **1998**, *17*, 786–788.
- (20) Roesky, P. W.; Gamer, M. T.; Marinos, N. Yttrium and Lanthanide Diphosphanylides: Syntheses and Structures of Complexes with one  $\{(\text{Ph}_2\text{P})_2\text{N}\}^-$  ligand in the Coordination Sphere. *Chem. - Eur. J.* **2004**, *10*, 3537–3542.
- (21) Poremba, P.; Edlmann, F. T. Cyclooctatetraenyl complexes of the early transition metals and lanthanides IX. (Cyclooctatetraenyl)-lanthanide diazadiene complexes. *J. Organomet. Chem.* **1997**, *549*, 101–104.
- (22) Panda, T. K.; Zulys, A.; Gamer, M. T.; Roesky, P. W. Cyclooctatetraene Complexes of Yttrium and the Lanthanides with Bis(phosphinimino)methanides: Synthesis, Structure, and Hydroamination/Cyclization Catalysis I. *Organometallics* **2005**, *24*, 2197–2202.
- (23) Zulys, A.; Panda, T. K.; Gamer, M. T.; Roesky, P. W. A samarium cyclooctatetraene complex as catalyst for hydroamination/cyclization catalysis. *Chem. Commun.* **2004**, 2584–2585.
- (24) Zhang, P.; Zhang, L.; Tang, J. Lanthanide single molecule magnets: progress and perspective. *Dalton Trans.* **2015**, *44*, 3923–3929.
- (25) Layfield, R. A. Organometallic Single-Molecule Magnets. *Organometallics* **2014**, *33*, 1084–1099.
- (26) Jeletic, M.; Lin, P.-H.; Le Roy, J. J.; Korobkov, I.; Gorelsky, S. I.; Murugesu, M. An Organometallic Sandwich Lanthanide Single-Ion Magnet with an Unusual Multiple Relaxation Mechanism. *J. Am. Chem. Soc.* **2011**, *133*, 19286–19289.
- (27) Jiang, S.-D.; Wang, B.-W.; Sun, H.-L.; Wang, Z.-M.; Gao, S. An Organometallic Single-Ion Magnet. *J. Am. Chem. Soc.* **2011**, *133*, 4730–4733.
- (28) Boulon, M.-E.; Cucinotta, G.; Liu, S.-S.; Jiang, S.-D.; Ungur, L.; Chibotaru, L. F.; Gao, S.; Sessoli, R. Angular-Resolved Magnetometry Beyond Triclinic Crystals: Out-of-Equilibrium Studies of  $\text{Cp}^*\text{ErCOT}$  Single-Molecule Magnet. *Chem. - Eur. J.* **2013**, *19*, 13726–13731.
- (29) Ungur, L.; Le Roy, J. J.; Korobkov, I.; Murugesu, M.; Chibotaru, L. F. Fine-tuning the Local Symmetry to Attain Record Blocking Temperature and Magnetic Remanence in a Single-Ion Magnet. *Angew. Chem., Int. Ed.* **2014**, *53*, 4413–4417.
- (30) Le Roy, J. J.; Ungur, L.; Korobkov, I.; Chibotaru, L. F.; Murugesu, M. Coupling Strategies to Enhance Single-Molecule Magnet Properties of Erbium–Cyclooctatetraenyl Complexes. *J. Am. Chem. Soc.* **2014**, *136*, 8003–8010.
- (31) Le Roy, J. J.; Korobkov, I.; Kim, J. E.; Schelter, E. J.; Murugesu, M. Structural and magnetic conformation of a cerocene  $[\text{Ce}(\text{COT}'')_2]^-$  exhibiting a uniconfigurational f1 ground state and slow-magnetic relaxation. *Dalton Trans.* **2014**, *43*, 2737–2740.
- (32) Le Roy, J. J.; Gorelsky, S. I.; Korobkov, I.; Murugesu, M. Slow Magnetic Relaxation in Uranium(III) and Neodymium(III) Cyclooctatetraenyl Complexes. *Organometallics* **2015**, *34*, 1415–1418.
- (33) Jiang, S.-D.; Wang, B.-W.; Su, G.; Wang, Z.-M.; Gao, S. A Mononuclear Dysprosium Complex Featuring Single-Molecule-Magnet Behavior. *Angew. Chem., Int. Ed.* **2010**, *49*, 7448–7451.
- (34) Liu, J.; Chen, Y.-C.; Liu, J.-L.; Vieru, V.; Ungur, L.; Jia, J.-H.; Chibotaru, L. F.; Lan, Y.; Wernsdorfer, W.; Gao, S.; Chen, X.-M.; Tong, M.-L. A Stable Pentagonal Bipyramidal Dy(III) Single-Ion Magnet with a Record Magnetization Reversal Barrier over 1000 K. *J. Am. Chem. Soc.* **2016**, *138*, 5441–5450.
- (35) Chen, S.-M.; Xiong, J.; Zhang, Y.-Q.; Yuan, Q.; Wang, B.-W.; Gao, S. A soft phosphorus atom to “harden” an Erbium(III) single-ion magnet. *Chem. Sci.* **2018**, *9*, 7540–7545.
- (36) Gregson, M.; Chilton, N. F.; Ariciu, A.-M.; Tuna, F.; Crowe, I. F.; Lewis, W.; Blake, A. J.; Collison, D.; McInnes, E. J. L.; Winpenny, R. E. P.; Liddle, S. T. A monometallic lanthanide bis(methanediide) single molecule magnet with a large energy barrier and complex spin relaxation behaviour. *Chem. Sci.* **2016**, *7*, 155–165.

- (37) Chilton, N. F.; Goodwin, C. A. P.; Mills, D. P.; Winpenny, R. E. P. The first near-linear bis(amide) f-block complex: a blueprint for a high temperature single molecule magnet. *Chem. Commun.* **2015**, *51*, 101–103.
- (38) Chilton, N. F. Design Criteria for High-Temperature Single-Molecule Magnets. *Inorg. Chem.* **2015**, *54*, 2097–2099.
- (39) Guo, F. S.; Day, B. M.; Chen, Y. C.; Tong, M. L.; Mansikkamäki, A.; Layfield, R. A. A Dysprosium Metallocene Single-Molecule Magnet Functioning at the Axial Limit. *Angew. Chem., Int. Ed.* **2017**, *56*, 11445–11449.
- (40) Goodwin, C. A. P.; Ortu, F.; Reta, D.; Chilton, N. F.; Mills, D. P. Molecular magnetic hysteresis at 60 K in dysprosocenium. *Nature* **2017**, *548*, 439.
- (41) Day, B. M.; Guo, F.-S.; Layfield, R. A. Cyclopentadienyl Ligands in Lanthanide Single-Molecule Magnets: One Ring To Rule Them All? *Acc. Chem. Res.* **2018**, *51*, 1880–1889.
- (42) Benndorf, P.; Kratsch, J.; Hartenstein, L.; Preuss, C. M.; Roesky, P. W. Chiral Benzamidinate Ligands in Rare-Earth-Metal Coordination Chemistry. *Chem. - Eur. J.* **2012**, *18*, 14454–14463.
- (43) Benndorf, P.; Jenter, J.; Zielke, L.; Roesky, P. W. Chiral lutetium benzamidinate complexes. *Chem. Commun.* **2011**, *47*, 2574–2576.
- (44) Kratsch, J.; Kuzdrowska, M.; Schmid, M.; Kazeminejad, N.; Kaub, C.; Oña-Burgos, P.; Guillaume, S. M.; Roesky, P. W. Chiral Rare Earth Borohydride Complexes Supported by Amidinate Ligands: Synthesis, Structure, and Catalytic Activity in the Ring-Opening Polymerization of rac-Lactide. *Organometallics* **2013**, *32*, 1230–1238.
- (45) Brunner, T. S.; Benndorf, P.; Gamer, M. T.; Knöfel, N.; Gugau, K.; Roesky, P. W. Enantiopure Amidinate Complexes of the Rare-Earth Elements. *Organometallics* **2016**, *35*, 3474–3487.
- (46) Benndorf, P.; Preuß, C.; Roesky, P. W. Synthesis of enantiomeric pure lithium and potassium benzamidinate complexes. *J. Organomet. Chem.* **2011**, *696*, 1150–1155.
- (47) Bodenstein, T. Entwicklung und Anwendung von Multi-referenzverfahren zur Beschreibung magnetischer Eigenschaften von Metallkomplexen. Dissertation, Karlsruher Institut für Technologie (KIT), 2015.
- (48) He, M. Synthesis of Chiral Rare Earth and Alkaline Earth Compounds: Magnetism and Catalytic Studies. Dissertation, Karlsruher Institut für Technologie (KIT), 2016.
- (49) Benndorf, P.; Kratsch, J.; Hartenstein, L.; Preuss, C. M.; Roesky, P. W. Chiral Benzamidinate Ligands in Rare-Earth-Metal Coordination Chemistry. *Chem. - Eur. J.* **2012**, *18*, 14454–14463.
- (50) Meihaus, K. R.; Long, J. R. Magnetic Blocking at 10 K and a Dipolar-Mediated Avalanche in Salts of the Bis( $\eta^8$ -cyclooctatetraene) Complex  $[\text{Er}(\text{COT})_2]^-$ . *J. Am. Chem. Soc.* **2013**, *135*, 17952–17957.
- (51) Jiang, S.-D.; Liu, S.-S.; Zhou, L.-N.; Wang, B.-W.; Wang, Z.-M.; Gao, S. Series of Lanthanide Organometallic Single-Ion Magnets. *Inorg. Chem.* **2012**, *51*, 3079–3087.
- (52) Brown, A. J.; Pinkowicz, D.; Saber, M. R.; Dunbar, K. R. A Trigonal-Pyramidal Erbium(III) Single-Molecule Magnet. *Angew. Chem., Int. Ed.* **2015**, *54*, 5864–5868.
- (53) Layfield, R. A.; McDouall, J. J. W.; Sulway, S. A.; Tuna, F.; Collison, D.; Winpenny, R. E. P. Influence of the N-Bridging Ligand on Magnetic Relaxation in an Organometallic Dysprosium Single-Molecule Magnet. *Chem. - Eur. J.* **2010**, *16*, 4442–4446.
- (54) Tang, J.; Hewitt, L.; Madhu, N. T.; Chastanet, G.; Wernsdorfer, W.; Anson, C. E.; Benelli, C.; Sessoli, R.; Powell, A. K. Dysprosium Triangles Showing Single-Molecule Magnet Behavior of Thermally Excited Spin States. *Angew. Chem.* **2006**, *118*, 1761–1765.
- (55) Gamer, M. T.; Lan, Y.; Roesky, P. W.; Powell, A. K.; Clérac, R. Pentanuclear Dysprosium Hydroxy Cluster Showing Single-Molecule-Magnet Behavior. *Inorg. Chem.* **2008**, *47*, 6581–6583.
- (56) Zheng, Y.-Z.; Lan, Y.; Anson, C. E.; Powell, A. K. Anion-Perturbed Magnetic Slow Relaxation in Planar  $\{\text{Dy}_4\}$  Clusters. *Inorg. Chem.* **2008**, *47*, 10813–10815.
- (57) Bi, Y.; Wang, X.-T.; Liao, W.; Wang, X.; Deng, R.; Zhang, H.; Gao, S. Thiacalix[4]arene-Supported Planar Ln<sub>4</sub> (Ln = TbIII, DyIII) Clusters: Toward Luminescent and Magnetic Bifunctional Materials. *Inorg. Chem.* **2009**, *48*, 11743–11747.
- (58) Abbas, G.; Lan, Y.; Kostakis, G. E.; Wernsdorfer, W.; Anson, C. E.; Powell, A. K. Series of Isostructural Planar Lanthanide Complexes  $[\text{LnIII}_4(\mu_3\text{-OH})_2(\text{mdeaH})_2(\text{piv})_6]$  with Single Molecule Magnet Behavior for the Dy<sub>4</sub> Analogue. *Inorg. Chem.* **2010**, *49*, 8067–8072.
- (59) Abragam, A.; Bleaney, B. *Electron Paramagnetic Resonance of Transition Ions*; Oxford University Press: Oxford, 2012; p 1–726.
- (60) Taylor, M. D.; Carter, C. P. Preparation of anhydrous lanthanide halides, especially iodides. *J. Inorg. Nucl. Chem.* **1962**, *24*, 387–391.
- (61) Coles, M. P. Application of neutral amidines and guanidines in coordination chemistry. *Dalton Trans.* **2006**, 985–1001.
- (62) Burton, N. C.; Cloke, F. G. N.; Joseph, S. C. P.; Karamallakis, H.; Sameh, A. A. Trimethylsilyl derivatives of cyclooctatetraene. *J. Organomet. Chem.* **1993**, *462*, 39–43.
- (63) Sheldrick, G. A short history of SHELX. *Acta Crystallogr., Sect. A: Found. Crystallogr.* **2008**, *64*, 112–122.
- (64) Sheldrick, G. Crystal structure refinement with SHELXL. *Acta Crystallogr., Sect. C: Struct. Chem.* **2015**, *71*, 3–8.
- (65) Dolomanov, O. V.; Bourhis, L. J.; Gildea, R. J.; Howard, J. A. K.; Puschmann, H. OLEX2: a complete structure solution, refinement and analysis program. *J. Appl. Crystallogr.* **2009**, *42*, 339–341.
- (66) Aquilante, F.; Autschbach, J.; Carlson, R. K.; Chibotaru, L. F.; Delcey, M. G.; De Vico, L.; Fdez. Galván, I.; Ferré, N.; Frutos, L. M.; Gagliardi, L. Molcas 8: New capabilities for multiconfigurational quantum chemical calculations across the periodic table. *J. Comput. Chem.* **2016**, *37*, 506–541.
- (67) Visscher, L.; Jensen, H. J. Aa.; Bast, R.; Saue, T.; Bakken, V.; Dyall, K. G.; Dubillard, S.; Ekstroem, U.; Eliav, E.; Enevoldsen, T.; Fasshauer, E.; Fleig, T.; Fossgaard, O.; Gomes, A. S. P.; Helgaker, T.; Henriksson, J.; Ilias, M.; Jacob, Ch. R.; Knecht, S.; Komorovsky, S.; Kullie, O.; Laerdahl, J. K.; Larsen, C. V.; Lee, Y. S.; Nataraj, H. S.; Nayak, M. K.; Norman, P.; Olejniczak, G.; Olsen, J.; Park, Y. C.; Pedersen, J. K.; Pernpointner, M.; Di Remigio, R.; Ruud, K.; Salek, P.; Schimmelpennig, B.; Sikkema, J.; Thorvaldsen, A. J.; Thyssen, J.; van Stralen, J.; Villaume, S.; Visser, O.; Winther, T.; Yamamoto, S. DIRAC16, a relativistic ab initio electronic structure program; DIRAC, 2016.
- (68) Widmark, P.-O.; Malmqvist, P.-Å.; Roos, B. O. Density matrix averaged atomic natural orbital (ANO) basis sets for correlated molecular wave functions. *Theor. Chim. Acta* **1990**, *77*, 291–306.
- (69) Roos, B. O.; Lindh, R.; Malmqvist, P.-Å.; Veryazov, V.; Widmark, P.-O. Main Group Atoms and Dimers Studied with a New Relativistic ANO Basis Set. *J. Phys. Chem. A* **2004**, *108*, 2851–2858.
- (70) Roos, B. O.; Lindh, R.; Malmqvist, P.-Å.; Veryazov, V.; Widmark, P.-O.; Borin, A. C. New Relativistic Atomic Natural Orbital Basis Sets for Lanthanide Atoms with Applications to the Ce Diatom and LuF<sub>3</sub>. *J. Phys. Chem. A* **2008**, *112*, 11431–11435.
- (71) Gomes, A. S. P.; Dyall, K. G.; Visscher, L. Relativistic double-zeta, triple-zeta, and quadruple-zeta basis sets for the lanthanides La–Lu. *Theor. Chem. Acc.* **2010**, *127*, 369–381.
- (72) Peng, D.; Reiher, M. Exact decoupling of the relativistic Fock operator. *Theor. Chem. Acc.* **2012**, *131*, 1081.
- (73) Roos, B. O.; Taylor, P. R.; Siegbahn, P. E. M. A complete active space SCF method (CASCF) using a density matrix formulated super-CI approach. *Chem. Phys.* **1980**, *48*, 157–173.
- (74) Parmar, P.; Peterson, K. A.; Clark, A. E. Static electric dipole polarizabilities of An<sup>5+/6+</sup> and AnO<sub>2</sub><sup>+/2+</sup> (An = U, Np, and Pu) ions. *J. Chem. Phys.* **2014**, *141*, 234304.
- (75) Andersson, K.; Malmqvist, P. A.; Roos, B. O.; Sadlej, A. J.; Wolinski, K. Second-order perturbation theory with a CASCF reference function. *J. Phys. Chem.* **1990**, *94*, 5483–5488.
- (76) Heß, B. A.; Marian, C. M.; Wahlgren, U.; Gropen, O. A mean-field spin-orbit method applicable to correlated wavefunctions. *Chem. Phys. Lett.* **1996**, *251*, 365–371.
- (77) Chibotaru, L. F.; Ungur, L.; Aronica, C.; Elmoll, H.; Pilet, G.; Luneau, D. Structure, Magnetism, and Theoretical Study of a Mixed-Valence CoII3CoIII4 Heptanuclear Wheel: Lack of SMM Behavior

despite Negative Magnetic Anisotropy. *J. Am. Chem. Soc.* **2008**, *130*, 12445–12455.

(78) Chibotaru, L. F.; Ungur, L. Ab initio calculation of anisotropic magnetic properties of complexes. I. Unique definition of pseudospin Hamiltonians and their derivation. *J. Chem. Phys.* **2012**, *137*, 064112.

(79) Mulliken, R. S. Electronic Population Analysis on LCAO–MO Molecular Wave Functions. I. *J. Chem. Phys.* **1955**, *23*, 1833–1840.